THE JOURNAL OF PHYSICAL CHEMISTRY B

pubs.acs.org/JPCB Article

Unraveling the Structural Dynamics of an Enzyme Encapsulated within a Metal−Organic Framework

T. N. A. Tuan Kob, M. F. Ismail, M. B. Abdul Rahman, Kyle E. Cordova, and M. A. Mohammad Latif*

Cite This: https://dx.doi.org/10.1021/acs.jpcb.0c02145 Read Online

ACCESS | Metrics & More | Article Recommendations | Supporting Information

ABSTRACT: Herein, we detail an atomic-level investigation of the cutinase enzyme encapsulated within a model metal−organic framework (MOF) platform using quantum mechanics calculations and molecular dynamics simulations. Cutinase, when encapsulated in an isoreticularly expanded MOF-74 (cutinase@IRMOF-74-VI), was proven to maintain its structural stability at temperatures that would otherwise denature the enzyme in its unprotected native state. Hydrogen bonding and salt bridge interactions, most notably involving arginine residues at the surface of the enzyme, were critical for stabilizing cutinase within the pore channels of IRMOF-74-VI. The findings reported support the viability of enzyme encapsulation in a porous material by demonstrating that a model enzyme not only retains its structural integrity but also remains accessible and active under extreme and foreign conditions.

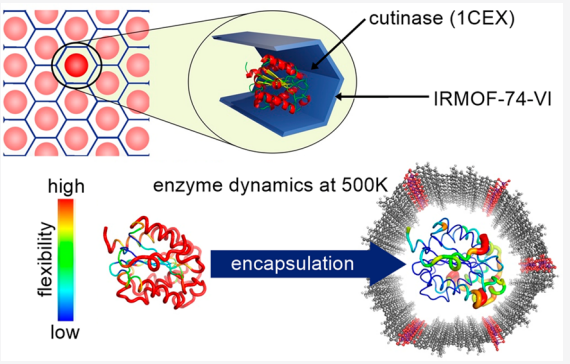

INTRODUCTION

Enzymes are nature's proven catalysts that, when exploited properly, produce relevant, value-added chemicals.[1] The past several decades have witnessed rapid improvements in enzymatic catalysis; however, the effectiveness of enzymes in industrial applications remains limited as a result of their low thermal stability, denaturation under practical conditions, and lack of efficient recovery processes.[2] It is well understood that enzyme encapsulation serves as a viable strategy for maintaining enzymatic function while at the same time protecting the catalyst from external perturbing factors.[3]

Metal−organic frameworks (MOFs) are a class of porous, crystalline materials that are recognized as ideal host platforms for encapsulating important enzymes.[4] Due to the modular nature of MOFs, several encapsulation strategies have been experimentally pursued and realized (e.g., surface attachment, covalent linkage, physical adsorption, and co-precipitation, to name a few).[5,6] In comparison with other "traditional" porous materials, such as mesoporous silica, sol−gel, and zeolites, MOFs are proving to be superior with respect to retaining the respective enzyme within its pores, thereby avoiding or, at the very least, significantly reducing leaching while at the same time effectively protecting the enzyme against denaturing media and elevated temperatures.[7−9] However, despite this promise the integrity, stability, catalytic activity, and efficiency of the enzyme remain at the mercy of the nature and outcome of the encapsulation process.[10] Accordingly, important information on how the encapsulated enzymes behave within the MOFs and what intermolecular interactions between them influence a given enzyme's structural stability once inside are scarcely available, with only a handful of reports seeking to understand this complex interplay at the molecular level.[11−13] One such important study came from Zhang et al., who employed molecular dynamics (MD) simulations in order to study the binding of amino acid side chain analogues with the internal surface of IRMOF-74-I (i.e., the parent MOF-74 structure).[13] Their results demonstrated that binding was primarily driven by van der Waals interactions, with the size of the guest molecules being the critical factor affecting the binding strength. In addition, a small protein, Trp-cage, was demonstrated to undergo denaturation when encapsulated by the IRMOF-74-VI. However, upon modulation of the polarity of the MOF's surface, Trp-cage's conformation was successfully maintained even at 400 K. It is suspected that larger enzymes, which possess stable inner-core conformations, will show strikingly different behavior when encapsulated within MOFs. This suspicion is in line with available experimental evidence that demonstrates that larger enzymes typically gain increased stability under extreme conditions in such circumstances.[7] However, the underlying molecular reasons for why this occurs have yet to be studied, and given the diversity of size, shape, and surface topologies among enzymes there is a real need for the further exploration of the structural dynamics of encapsulated enzymes. Such information would inevitably

Received: March 10, 2020
Revised: April 3, 2020
Published: April 10, 2020

provide a much-needed blueprint for judiciously choosing the appropriate MOF platforms that meet the needs of the specific enzymes to be encapsulated.

In this report, we detail an atomic-level investigation of a large enzyme, cutinase, encapsulated within a model MOF platform using quantum mechanics calculations and MD simulations. Cutinase was chosen as the model enzyme due to its widespread relevance in the biodegradation of plastics, the production of renewable polyesters, the treatment of cotton fabrics, and food treatment and flavoring.[14−18] Similarly, the isoreticularly expanded MOF-74 (IRMOF-74-VI) was chosen due to its remarkably high stability and surface area as well as its appropriately sized pore aperture (~4 × 5 nm).[19] By employing the relevant computational techniques in regard to this system, we were able to demonstrate the properties and behavior of cutinase when encapsulated within IRMOF-74-VI. Indeed, the reduced atomic displacement and atomic fluctuation of cutinase within IRMOF-74-VI at high temperatures indicated that its thermal stability was largely improved and, due to the atomic-level investigation, critical insights were gleamed regarding the specific interactions that were the primary contributors toward maintaining the stability.

COMPUTATIONAL DETAILS

Model Construction and Potential Function. The model construction of IRMOF-74-VI was based on its crystal structure.[19] The material's crystallographic information file was obtained from the Cambridge Crystallography Data Centre (CCDC code: 841647). IRMOF-74-VI crystallizes in the trigonal space group *R*3 (no. 146) with lattice parameters $a = b = 78.643$ Å and $c = 6.816$ Å and a unit cell volume of 36505.5 Å^3. The initial coordinates used to construct the cutinase model were also based on data from its crystal structure, which was obtained from the RCSB Protein Data Bank (PDB code: 1CEX). It is noted that the water molecules present in the crystal structure of cutinase were removed prior to carrying out the simulations. The topology of IRMOF-74-VI was generated using OBGMX, a web-based generator for GROMACS topology, and the AmberFF99sb-ILDN force field simulation was employed in order to describe the energy for all simulations.[20,21] Amber force fields are among the most commonly used in MD simulations for MOFs.[22]

Atomic Charge Derivation. Density functional theory (DFT) calculations were performed with the Gaussian 09 software package using the crystal structure of IRMOF-74-VI in order to determine the charge distribution among each atom in the MOF structure.[23] These single-point calculations were performed using the 6-31+g* basis set, which includes one polarization (*) and one diffuse (+) function on all atoms with the exception of hydrogen. The employed method produced charges that fit an electrostatic potential at specific points, which were selected according to the CHELPG scheme.[24] More detailed information on the interaction function force field and the atomic charge calculations (and deviations thereof) are provided in the Supporting Information, section S3.[25,26]

Molecular Dynamics Simulations. All MD simulations were performed using the GROMACS software (v 5.1.4) with the rigid TIP3P water model and AMBER99SB-ILDN force field simulation.[27,28] Cutinase was simulated in a cubic box with a periodic distance of 1.0 nm and filled with 11 392 water molecules. Periodic boundary conditions were applied in all directions. Two Cl^- ions were added in order to neutralize the net charge of the system. Covalent bonds to the hydrogen atoms were constrained using the LINCS algorithm, and long electrostatic interactions were treated by the particle mesh Ewald (PME) method.[29,30] Long-range van der Waals and electrostatic interactions were cut off at 1.0 nm. The leapfrog algorithm was used for potential energy integration at 2 fs intervals. The force field parameters of IRMOF-74-VI were validated by MD simulations in water for 5 ns under isothermal−isobaric conditions. The simulation was used in order to calculate the root-mean-square deviation (RMSD) of the simulated IRMOF-74-VI from the crystal structure. For cutinase@IRMOF-74-VI, a periodic simulation cell consisting of IRMOF-74-VI, cutinase, and water molecules was used. Initially, the energy minimization was conducted using the steepest-descent method with a maximum step size of 0.01 nm and a force tolerance of 10 kJ mol^{-1} nm^{-1}. Next, the velocities were assigned according to the Maxwell−Boltzmann distribution at 300 K. Covalent bonds to the hydrogen atoms were constrained using the LINCS algorithm, and long electrostatic interactions were calculated by the PME method. The cutoff for the long-range van der Waals and electrostatic interactions was set at 1.0 nm, and the time step was set to 2 fs. Each system was examined at five temperatures (300, 350, 400, 450, and 500 K). The temperature was controlled using the velocity-rescaling method with a temperature coupling constant of 0.1 ps.[31] The pressure was coupled using Parrinello−Rahman's barostat at 1 atm.[31] An anisotropic pressure coupling with a large constant of 20 ps was applied in order to better control the pressure for simulations of periodic IRMOF-74-VI. The MOF was considered to be rigid; hence, the framework atoms were position-restrained during the energy minimization and MD simulations. During the simulations, the IRMOF-74-VI unit cells coupled themselves through periodic boundary conditions. The systems were equilibrated in order by 500 ps of canonical and isothermal−isobaric ensemble MD simulations. The second step was repeated until a consistent plot of the potential energy was achieved. The equilibrated systems were then subjected to 50 ns of MD simulation (production) in an isothermal−isobaric ensemble.

RESULTS AND DISCUSSION

The primary objective of this research program was to understand the interplay among the enzyme, cutinase, and the chosen metal−organic framework support at the atomic level. It is our goal that, with the insights gleaned from this study, informed decision making can then take place as to which molecular interactions must be considered when developing new enzyme−MOF systems.

Tertiary Structural Stability and Flexibility of Cutinase@IRMOF-74-VI. The average atomic displacement profiles for cutinase in its native state (denoted herein as "free cutinase") and encapsulated cutinase (denoted herein as "cutinase@IRMOF-74-VI") at five different temperatures (300, 350, 400, 450, and 500 K) are shown in Figure 1. At 300 K, cutinase remained in its most stable conformation regardless of encapsulation, as evidenced by the average RMSD values calculated for free cutinase (0.158 ± 0.017 nm) and cutinase@IRMOF-74-VI (0.139 ± 0.007 nm). Our results agree with previous theoretical and experimental studies that showed RMSD values of 0.13 nm when the cutinase structure reaches a steady state at 300 K.[32,33] When increasing the temperature from 300 to 500 K, the average RMSD values also

https://dx.doi.org/10.1021/acs.jpcb.0c02145
J. Phys. Chem. B XXXX, XXX, XXX−XXX

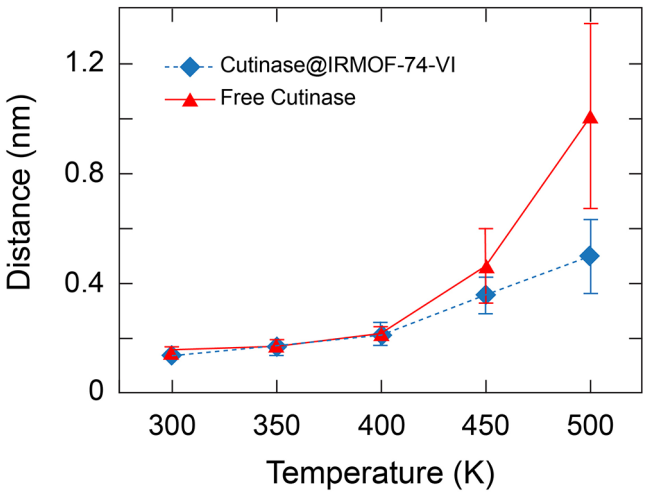

Figure 1. RMSD values that resulted from the MD simulations. The RMSD is shown for free cutinase (red triangles) and cutinase@IRMOF-74-VI (blue diamonds) in water as a function of time at different temperatures. Data were averaged from the last 10 ns of 50 ns MD simulations. Included error bars indicate uncertainty.

increased. Based on these values, a considerable change in the atomic displacement profiles was observed when the temperature increased above the optimum temperature for free cutinase (450−500 K).[34] Although both systems exhibited increases in their RMSD values as a function of the increasing temperature, the increase in values for cutinase@IRMOF-74-VI within 50 ns of the MD simulation was significantly lower. At 500 K, cutinase@IRMOF-74-VI (0.500 ± 0.133 nm) produced a 0.51 nm-lower RMSD value than free cutinase (1.011 ± 0.334 nm).

The trends in the behavior of the average RMSD values for both sets of simulations are a consequence of the enhanced motion between the atoms in the systems. It is noted that the average kinetic energy of both systems at 500 K was calculated to be 1.540×10^5 and 1.399×10^5 kJ mol^{-1} for free cutinase and cutinase@IRMOF-74-VI, respectively. Indeed, the lower average kinetic energy of cutinase@IRMOF-74-VI corresponds to less structural motion between the atoms compared to a scenario where cutinase is in its unprotected native state. These results from 50 ns of MD simulations already provided clear evidence that IRMOF-74-VI plays an important role in restricting the atomic displacement of cutinase's underlying structure at elevated temperatures, which in turn means that the enzyme's stability and activity have the potential to be maintained over a wider range of conditions.

In order to further explore the stability of cutinase in its native and encapsulated forms, the atomic fluctuations of each amino acid residue were investigated as functions of temperature. Specifically, in order to gain a deeper understanding of the conformational flexibility of cutinase, the root-mean-square fluctuations (RMSFs) of each amino acid residue were plotted by exploiting the interatomic displacement between each amino acid residue in the cutinase structure. As expected, the overall atomic fluctuations increased when the temperature was increased for both free cutinase and cutinase@IRMOF-74-VI. As shown in Figure 2a, the loop regions of free cutinase (amino acid residues 17−33) as well as the N-terminal region and loop (residues 212 and 213, respectively) fluctuated at slightly higher levels than the other residues. As the temperature increased from 300 to 500 K, the fluctuations

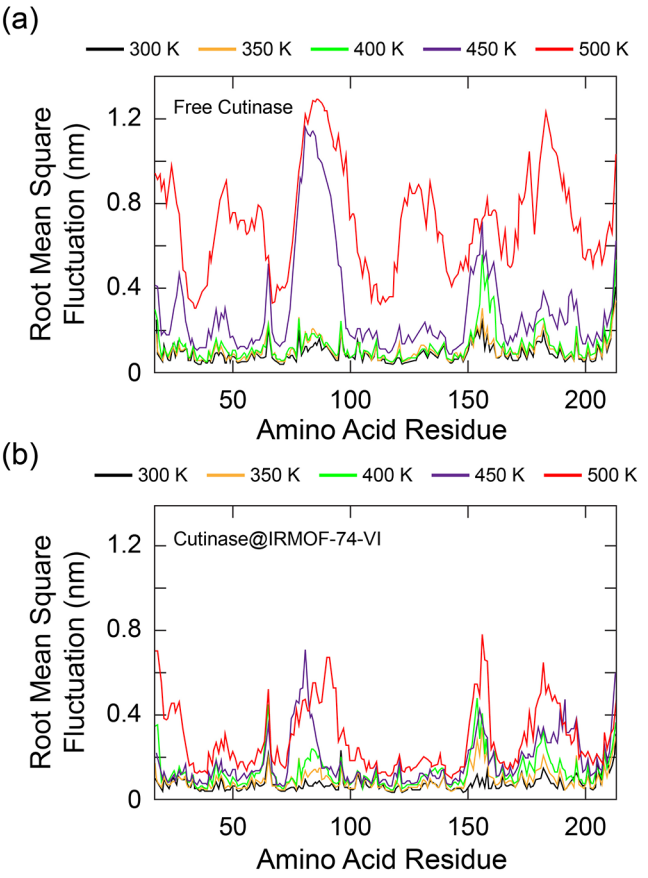

Figure 2. Root-mean-square fluctuations (RMSFs) resulting from the MD simulations. The RMSFs for (a) free cutinase and (b) cutinase@IRMOF-74-VI are shown as functions of time at temperatures from 300 to 500 K. The RMSFs of the amino acid residues were calculated from a 0 to 50 ns simulation time. The RMSF results for temperatures of 300, 350, 400, 450, and 500 K are colored black, yellow, green, purple, and red, respectively.

became significantly more pronounced and were nearly double the RMSF values obtained for the same regions when cutinase was encapsulated within IRMOF-74-VI (Figure 2b).

At 500 K, the fluctuation differences were at their most extreme. This finding strongly indicates that using IRMOF-74-VI as a support stabilizes the cutinase structure and function. In the cutinase tertiary structure, two flexible loops (residues 80−90 and 182−189) bearing hydrophobic amino acids constitute the binding site of the enzyme.[32] As such, these two loops have an ample amount of anisotropy and exhibit flexibility in order to allow for meaningful interactions to occur with prospective substrates.[32] From our MD simulations, these regions did, in fact, display a degree of flexibility. However, IRMOF-74-VI was determined to reduce the atomic fluctuations of these regions at higher temperatures; this finding is favorable in terms of enhancing the structural stability while retaining the ability of cutinase to interact with a given substrate without denaturing (Figure 2).

A useful measure of the enzyme dynamics is the theoretical *B*-factor, whose value reflects the fluctuation of atoms about their average position. As such, the theoretical *B*-factor was calculated for each amino acid residue in free cutinase and cutinase@IRMOF-74-VI (Table S7). The *B*-factor values were also found to increase as a function of temperature. In agreement with the trends in the RMSD and RMSF values, the

https://dx.doi.org/10.1021/acs.jpcb.0c02145
J. Phys. Chem. B XXXX, XXX, XXX−XXX

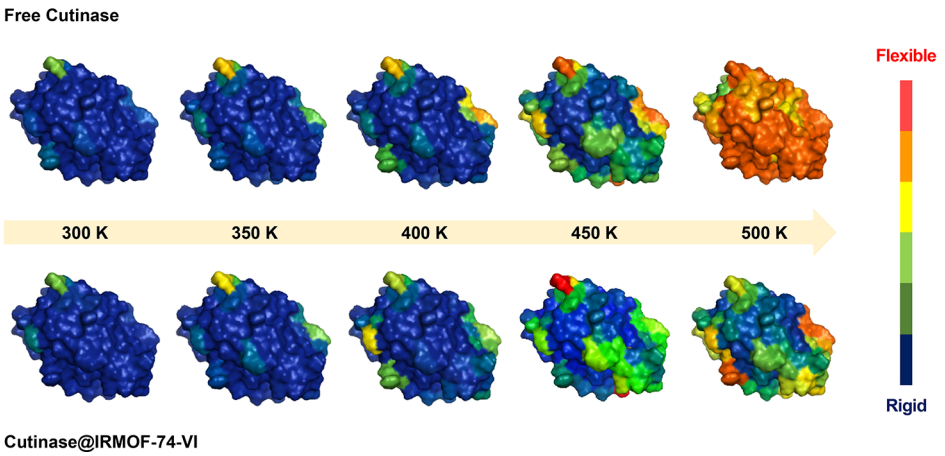

Figure 3. The residual RMSFs were converted to theoretical *B*-factors and rendered using a spectrum of colors. Dark blue indicates the lowest structural flexibility (rigid), and red denotes the highest structural flexibility (flexible).

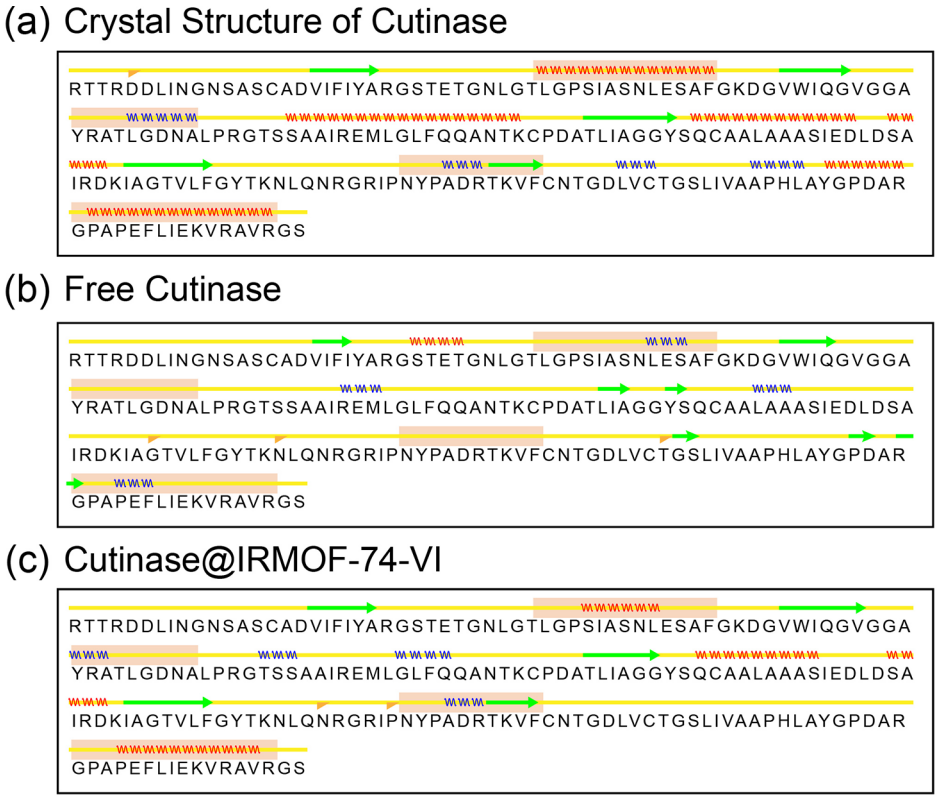

Figure 4. Secondary structural analysis of cutinase. The underlying structural elements are shown for cutinase in (a) its ideal crystal structure form, (b) its free native state, and (c) encapsulated within IRMOF-74-VI. Note that these structural changes were observed after 50 ns of molecular dynamics simulations. The amino acid numbering is sequential from Arg17 to Ser213. The colors in the graphs correspond to the bridge (yellow with an arrow), α-helix (red), π-helix (green), 3−10 helix (blue), and coil and turn (yellow).

B-factor values were lower for cutinase@IRMOF-74-VI than free cutinase. As presented in Figure 3, higher *B*-factor values were observed at specific regions of the enzyme's structure. These regions (residues 96, 151, 154, 156, and 182) are consistent with the residues that were previously demonstrated to produce the highest fluctuations in the atomic position (Figure 2a and b).

Secondary Structure Analysis. In order to gain a better understanding of the structural dynamics, the STRIDE algorithm was employed in order to assess the elements of the secondary structure of cutinase.[35] As illustrated in Figure 4, the free cutinase structure experienced extensive changes in its secondary structural elements when placed in water at 500 K. In general, when cutinase was encapsulated within IRMOF-74-VI, the secondary structure was retained at a higher degree than for free cutinase. Throughout the MD simulations, the percentage of helices was found to remain higher for cutinase@IRMOF-74-VI at temperatures below 500 K. It is noted that the secondary structural profiles for all the systems studied are available in the Supporting Information, Figure S11. As shown in Figure 4, the majority of the α-helices were maintained for cutinase@IRMOF-74-VI at 500 K, and only a slight reduction in the helicity of residues 51−53 and 60−63 was observed. In comparison, the free cutinase lost α-helices at

https://dx.doi.org/10.1021/acs.jpcb.0c02145
J. Phys. Chem. B XXXX, XXX, XXX−XXX

450 K (residues 164−166). This loss of α-helices was even more prominent at 500 K, at which point almost all the α-helices were absent with the exception of residues 96−98. These residues formed a hydrophobic core and appeared to be remarkably stable despite the thermal unfolding.

The average fraction of α-helices in free cutinase and cutinase@IRMOF-74-VI and the distance between the two amino acid ends of cutinase (D_{end}) were used in order to further evaluate the enzyme's secondary structure (Figure 5).

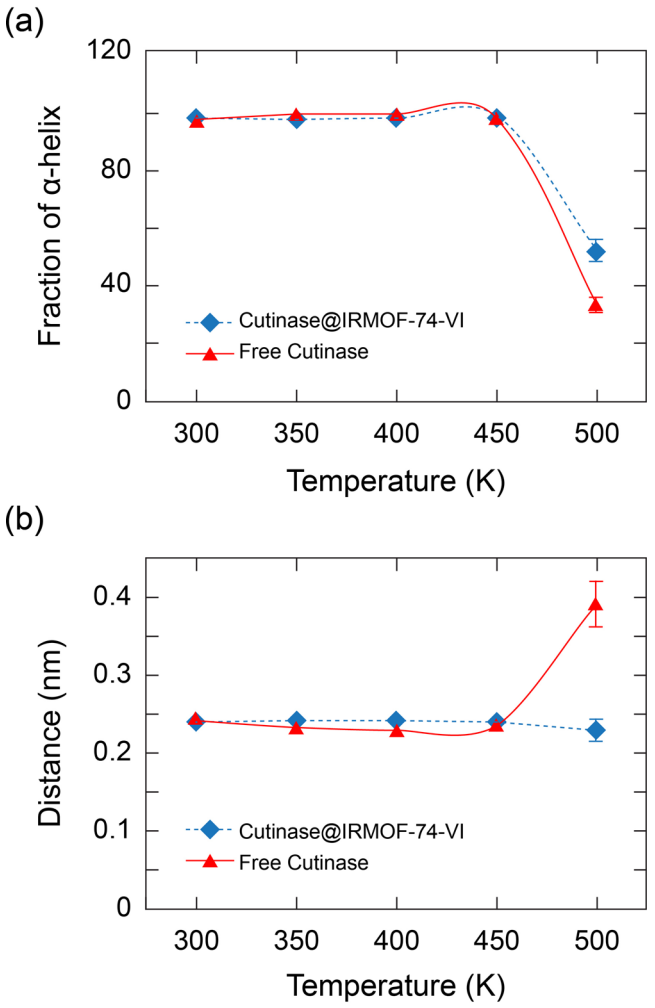

Figure 5. Secondary structural analyses from the molecular dynamic simulations. (a) The fraction of α-helices in free cutinase (red triangles) and cutinase@IRMOF-74-VI (blue diamonds). (b) The distance (D_{end}) between the two ends of cutinase's secondary structure as a function of temperature.

The fraction of α-helices for free cutinase decreased from 97.6 at 300 K to 33.5 at 500 K. At temperatures higher than 450 K, there was an abrupt decrease in the fraction of α-helices, whereas the D_{end} values increased. These results indicate that free cutinase was already unfolded during the 50 ns MD simulation at 450 K. For cutinase@IRMOF-74-VI, a higher secondary structure stability was apparent. Although cutinase@IRMOF-74-VI exhibited a high level of dissociation of α-helices, there was less detachment of the remaining α-helices from the other loops.

Using the STRIDE algorithm, the total solvent accessible surface areas (SASAs) of free cutinase and cutinase@IRMOF-74-VI were calculated as a function of temperature.[35] In general, the total SASAs for each system increased proportionally with temperature (Table S8). For all the temperatures investigated, the interactions between cutinase and IRMOF-74-VI reduced the total SASA. The hydrophobic interactions are of particular interest given the hydrophobic nature of IRMOF-74-VI, since its organic linker, which contains six phenylene rings, forms the basis of the pore channels. The hydrophobic SASA value for free cutinase remained relatively constant from 300 to 450 K but suddenly increased by 73% when the temperature increased from 450 to 500 K. For the encapsulated cutinase, the hydrophobic SASA value was higher overall than for free cutinase as the temperature increased from 350 to 450 K; however, this SASA value did not experience the same sudden increase (19.3%) when the temperature increased from 450 to 500 K. This finding again demonstrates the capability of IRMOF-74-VI to stabilize the enzyme's structure at temperatures that would otherwise would denature it.

Enzyme-MOF Interactions. Table 1 lists the specific interactions that occur when cutinase is encapsulated within IRMOF-74-VI at temperatures from 300 to 500 K. The focus here is the interactions between the pore walls of IRMOF-74-VI and the residues at the surface of cutinase. Here, the most dominant interactions were hydrophobic and increased with temperature (Table 1). This finding is consistent with the outcomes from the SASA analyses (Tables S8 and S9). From these results, it was clear that hydrophobic interactions provided the greatest contribution to binding specificity and strength in the cutinase@IRMOF-74-VI system. It is noted that arginine (Arg) was the amino acid residue most involved in the interactions between cutinase and IRMOF-74-VI.

It is known that certain amino acid residues that are commonly located at the surface of cutinase (e.g., Arg, Lys, Asp, and Glu) are able to form multiple interactions with an external species.[36] When comparing these residues, the unique geometric features of Arg's side chain afford it the ability to contribute more toward cutinase's structural stability. Arg is an

Table 1. Specific Interactions Formed between the Amino Acid Residues of Cutinase and IRMOF-74-VI at Various Temperatures

interactions	300 (K)	350 (K)	400 (K)	450 (K)	500 (K)
H-bonding	Arg96	Arg158, Thr173	Arg78	Arg158, Arg196, Asn27, Arg96	Arg158, Arg96, Asn27
hydrophobic	Pro193, Thr45, Arg17, Ile24	Pro187, Pro160, Pro193, Asn161, Asn27	Ile183, Ala190, Ala93, Asn161, Leu189, Pro193, Ala91, Pro198, Thr45, Ala136, Arg196	Ala79, Asn84, Ala185, Ala186, Ala79, Pro187, Leu189, Arg96, Leu153, Lys108, Ala29, Thr80, Pro193, Arg78, Asn161, Pro193	Pro87, Pro187, Ala85, Pro87, Thr90, Leu182, Leu189, Thr43, Leu51, Ala85, Leu86, Asn172, Leu189, Thr45, Leu101, Arg196, Ala209, Ile24
salt bridges	Arg96	Arg158	Arg78	Arg196, Arg158	Arg96, Arg158
π-cation	Arg156	Arg156, Arg96			Arg196

https://dx.doi.org/10.1021/acs.jpcb.0c02145
J. Phys. Chem. B XXXX, XXX, XXX−XXX

amphipathic amino acid with a hydrophobic side chain and a positively charged guanidinium group at the end of its structure. The guanidinium is exposed to the surface, while the hydrophobic portion is buried within the structure.[37] For this reason, Arg residues are found in a higher concentration at the surface of cutinase than other similarly related amino acids and, as such, are involved to a greater degree in the interactions with IRMOF-74-VI when cutinase is encapsulated (Figure S17). Specifically, Arg's positive charge is delocalized on the guanidinium group, which allows for the formation of hydrogen bonds (H-bonds) through interactions with the oxygen atoms of IRMOF-74-VI's linker. Furthermore, the guanidinium group on Arg has the exclusive ability to form H-bonds with water molecules that also exist within IRMOF-74-VI. It is also noted that the guanidinium group in arginine introduces interactions in three possible directions through its three asymmetrical nitrogen atoms, which allows arginine to form a large number of electrostatic interactions.[37] Indeed, these unique geometric features of Arg enable the residue to contribute to the structural stability of cutinase when encapsulated.[38]

For all the MD simulations performed, Arg formed at least one H-bond with IRMOF-74-VI (e.g., Arg96-O, Arg158-O, and Arg196-O) on average. These H-bond interactions have significant effects on the stabilization of the cutinase structure. Salt bridges are the result of a combination of H-bonds and electrostatic interactions.[39] Both H-bonds and salt bridges are important for maintaining cutinase's structural stability for its catalytic activity.[40] In our simulations, we observed that the salt bridge interactions increased proportionally with temperature. As presented in Table 1, strong interactions between the Arg158 residue and the O atom of the IRMOF-74-VI linker were found at 350, 450, and 500 K. It is worth noting that an Arg residue appeared in all the salt bridge interactions that arose from both strong and weak interactions (e.g., Arg158 at 350 K, Arg158 at 450 K, and Arg158 at 500 K). Previous theoretical and experimental studies have shown that π-cation interactions are capable of being quite strong, both in the gas phase and in the aqueous phase.[41] In total, four π-cation interactions were formed at 300, 350, and 500 K within the cutinase@IRMOF-74-VI model. Interestingly, there were no π-cation interactions found at 400 and 450 K. The π-cation interactions were formed mostly between the positively charged Arg residues and the aromatic ring of the MOF linker. The strongest π-cation interaction found in this study was between Arg156 and the MOF linker, with a distance of 5.31 Å.

In order to conceptually understand the specific interactions between certain amino acid residues of cutinase and specific atoms of IRMOF-74-VI, a correlation "heat" map was constructed (Figure 6). As shown, the "heat" map describes which interactions remained consistent throughout the 50 ns MD simulations. One of the most dominant interactions observed was between the Arg96 residue and the oxygen atom of the MOF linker. Furthermore, the interaction between the Arg156 residue and the CA atom of IRMOF-74-VI (an sp^3 carbon bonded to an sp^2 aromatic carbon) also showed a significant interaction strength. The results obtained from the correlation "heat" map agree with Table 1 in that the Arg residue was the primary contributor to the maintenance of cutinase's stability and functionality when encapsulated within IRMOF-74-VI, even at extreme temperatures.

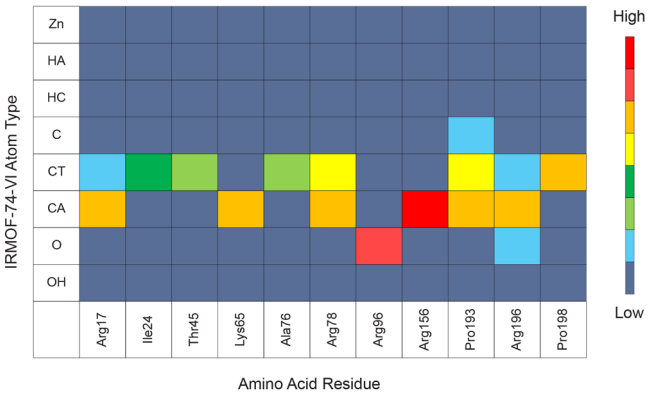

Figure 6. Correlation "heat" map for understanding the interactions between cutinase and IRMOF-74-VI at 300 K as a function of time (50 ns). Dark blue indicates few, if any, interactions, and red denotes the strongest interactions. The atom type code is as follows: Zn, zinc atom; CA, sp^2 aromatic carbon; HA, aromatic hydrogen bonded to CA; OH, hydroxyl oxygen; C, sp^2 carbon bonded to oxygen; O, oxygen bonded to sp^2 carbon; CT, sp^3 carbon bonded to CA; and HC, hydrogen atom bonded to CT.

CONCLUSION

The structural dynamics and properties of the cutinase enzyme encapsulated in IRMOF-74-VI were investigated by MD simulations at five different temperatures. Upon encapsulation, cutinase@IRMOF-74-VI exhibited a higher structural stability with smaller thermal fluctuations at elevated temperatures. During 50 ns of the MD simulations, cutinase retained a larger portion of its secondary structure even at temperatures reaching 500 K, whereas free cutinase had already denatured. The surface activity of the encapsulated cutinase was mostly hydrophobic. IRMOF-74-VI's pore walls consisted of hydrophobic linkers that interacted with the hydrophobic amino acid residues of cutinase. Most of the interactions identified originated from the Arg residues at the surface of the protein. The interactions created by Arg were mostly hydrophobic, i.e., H-bonding and salt bridges. It is important to note that there was no evidence of metal ion involvement from IRMOF-74-VI in regard to stabilizing the protein structure. IRMOF-74-VI showed that it could provide a suitable environment for protecting cutinase, which led to an improvement in the stability of the enzyme with an optimum range of interaction strengths that prevented enzyme denaturation at extreme temperatures. This indicates that the selective encapsulation of large biomolecules, such as enzymes, can be achieved using mesoporous MOFs with suitable pore sizes, appropriate internal pore environments, and proper organic linker utilizations. More atomic-level investigations of different biomolecules are needed with different MOFs in order to unravel the otherwise unknown behaviors or interactions that occur when targeting potential biocomposites. Such information will significantly contribute to the properly informed utilization of these porous materials for biological applications.

ASSOCIATED CONTENT

Supporting Information

The Supporting Information is available free of charge at https://pubs.acs.org/doi/10.1021/acs.jpcb.0c02145.

Supporting details on the IRMOF studied along with details concerning the computational methods employed (PDF)

https://dx.doi.org/10.1021/acs.jpcb.0c02145
J. Phys. Chem. B XXXX, XXX, XXX−XXX

AUTHOR INFORMATION

Corresponding Author

M. A. Mohammad Latif − *Integrated Chemical BioPhysics Research, Faculty of Science, Department of Chemistry, Faculty of Science, Centre of Foundation Studies for Agricultural Science, and Foundry of Reticular Materials for Sustainability (FORMS), Universiti Putra Malaysia, 43400 UPM Serdang, Selangor, Malaysia;* orcid.org/0000-0002-3345-0265; Email: aliflatif@upm.edu.my

Authors

T. N. A. Tuan Kob − *Integrated Chemical BioPhysics Research, Faculty of Science and Department of Chemistry, Faculty of Science, Universiti Putra Malaysia, 43400 UPM Serdang, Selangor, Malaysia*

M. F. Ismail − *Integrated Chemical BioPhysics Research, Faculty of Science and Department of Chemistry, Faculty of Science, Universiti Putra Malaysia, 43400 UPM Serdang, Selangor, Malaysia*

M. B. Abdul Rahman − *Integrated Chemical BioPhysics Research, Faculty of Science, Department of Chemistry, Faculty of Science, and Foundry of Reticular Materials for Sustainability (FORMS), Universiti Putra Malaysia, 43400 UPM Serdang, Selangor, Malaysia*

Kyle E. Cordova − *Department of Chemistry and Berkeley Global Science Institute, University of California—Berkeley, Berkeley, California 94720, United States; Materials Discovery Research Unit, Reticular Foundry, Royal Scientific Society, Amman 11941, Jordan;* orcid.org/0000-0002-4988-0497

Complete contact information is available at: https://pubs.acs.org/10.1021/acs.jpcb.0c02145

Notes

The authors declare no competing financial interest.

ACKNOWLEDGMENTS

The authors acknowledge the Ministry of Education Malaysia for the financial support provided under the Fundamental Research Grant Scheme (no. FRGS/1/2017/STG04/UPM/02/5). We are grateful to Prof. Omar M. Yaghi (U.C. Berkeley) for his support of global scientific activities.

REFERENCES

(1) Chen, S.; Su, L.; Chen, J.; Wu, J. Cutinase: Characteristics, preparation, and application. *Biotechnol. Adv.* **2013**, *31*, 1754−1767.

(2) Chapman, J.; Ismail, E. A.; Dinu, C. Z. Industrial applications of enzymes: Recent advances, techniques, and outlooks. *Catalysts* **2018**, *8* (6), 238.

(3) Es, I.; Vieira, J. D. G.; Amaral, A. C. Principles, techniques, and applications of biocatalyst immobilization for industrial application. *Appl. Microbiol. Biotechnol.* **2015**, *99* (5), 2065−2082.

(4) Drout, R. J.; Robison, L.; Farha, O. K. Catalytic applications of enzymes encapsulated in metal-organic frameworks. *Coord. Chem. Rev.* **2019**, *381*, 151−160.

(5) Lian, X.; Fang, Y.; Joseph, E.; Wang, Q.; Li, J.; Banerjee, S.; Lollar, C.; Wang, X.; Zhou, H. Enzyme MOF (metal-organic framework) composites. *Chem. Soc. Rev.* **2017**, *46*, 3386−3401.

(6) An, H.; Li, M.; Gao, J.; Zhang, Z.; Ma, S.; Chen, Y. Incorporation of biomolecules in metal-organic frameworks for advanced applications. *Coord. Chem. Rev.* **2019**, *384*, 90−106.

(7) Liang, K.; Ricco, R.; Doherty, C. M.; Styles, M. J.; Bell, S.; Kirby, N.; Mudie, S.; Haylock, D.; Hill, A. J.; Doonan, C. J.; Falcaro, P.; et al. Biomimetic mineralization of metal-organic frameworks as protective coatings for biomacromolecules. *Nat. Commun.* **2015**, *6*, 1−8.

(8) Li, P.; Modica, J. A.; Howarth, A. J.; Vargas L, E.; Moghadam, P. Z.; Snurr, R. Q.; Mrksich, M.; Hupp, J. T.; Farha, O. K. Toward design rules for enzyme immobilization in hierarchical mesoporous metal-organic frameworks. *Chem.* **2016**, *1*, 154−169.

(9) Liao, F.; Lo, W.; Hsu, Y.; Wu, C.; Wang, S.; Shieh, F.; Morabito, J. V.; Chou, L.; Wu, K. C.; Tsung, C. Shielding against unfolding by embedding enzymes in metal-organic frameworks via a de novo approach. *J. Am. Chem. Soc.* **2017**, *139*, 6530−6533.

(10) Betancor, L.; Luckarift, H. R. Bioinspired enzyme encapsulation for biocatalysis. *Trends Biotechnol.* **2008**, *26*, 566−572.

(11) Bilal, M.; Adeel, M.; Rasheed, T.; Iqbal, M. N. Multifunctional metal-organic frameworks-based biocatalytic platforms: Recent developments and future prospects. *J. Mater. Res. Technol.* **2019**, *8*, 2359−2371.

(12) Hu, Z.; Jiang, J. A helical peptide confined in metal-organic frameworks: Microscopic insight from molecular simulation. *Microporous Mesoporous Mater.* **2016**, *232*, 138−142.

(13) Zhang, H.; Lv, Y.; Tan, T.; van der Spoel, D. Atomistic simulation of protein encapsulation in metal-organic frameworks. *J. Phys. Chem. B* **2016**, *120*, 477−484.

(14) Ping, L. F.; Chen, X. Y.; Yuan, X. L.; Zhang, M.; Chai, Y. J.; Shan, S. D. Application and comparison in bio-synthesis and biodegradation by *Fusarium solani* and *Aspergillus fumigatus* cutinases. *Int. J. Biol. Macromol.* **2017**, *104*, 1238−1245.

(15) Hu, X.; Gao, Z.; Wang, Z.; Su, T.; Yang, L.; Li, P. Enzymatic degradation of poly(butylene succinate) by cutinase cloned from *Fusarium solani*. *Polym. Degrad. Stab.* **2016**, *134*, 211−219.

(16) Lee, S. H.; Song, W. S.; Kim, H. R. Cutinase treatment of cotton fabrics. *Fibers Polym.* **2009**, *10*, 802−806.

(17) Ferrario, V.; Pellis, A.; Cespugli, M.; Guebitz, G. M.; Gardossi, L. Nature inspired solutions for polymers: Will cutinase enzymes make polyesters and polyamides greener. *Catalysts* **2016**, *6*, 205.

(18) Nikolaivits, E.; Makris, G.; Topakas, E. Immobilization of a cutinase from *Fusarium oxysporum* and application in pineapple flavor synthesis. *J. Agric. Food Chem.* **2017**, *65*, 3505−351.

(19) Deng, H.; Grunder, S.; Cordova, K. E.; Valente, C.; Furukawa, H.; Hmadeh, M.; Gándara, F.; Whalley, A. C.; Liu, Z.; Asahina, S.; et al. Large-pore apertures in a series of metal-organic frameworks. *Science* **2012**, *336*, 1018−1023.

(20) Garberoglio, G. OBGMX: A web-based generator of GROMACS topologies for molecular and periodic systems using the universal force field. *J. Comput. Chem.* **2012**, *33*, 2204−2208.

(21) Lindorff-Larsen, K.; Piana, S.; Palmo, K.; Maragakis, P.; Klepeis, J. L.; Dror, R. O.; Shaw, D. E. Improved side-chain torsion potentials for the Amber ff99SB protein force field. *Protein.* **2010**, *78* (8), 1950−1958.

(22) Zheng, B.; Sant, M.; Demontis, P.; Suffritti, G. B. Force field for molecular dynamics computations in flexible ZIF-8 framework. *J. Phys. Chem. C* **2012**, *116* (1), 933−938.

(23) Frisch, M. J.; Trucks, G. W.; Schlegel, H. B.; Scuseria, G. E.; Robb, M. A.; Cheeseman Scalmani, J. R. G.; Barone, V.; Mennucci, B.; Petersson, G. A.; et al. *Gaussian 09*, rev. A.1; Gaussian, Inc.: Wallingford, CT, 2009.

(24) Breneman, C. M.; Wiberg, K. B. Determining atom-centered monopoles from molecular electrostatic potentials. The need for high sampling density in formamide conformational analysis. *J. Comput. Chem.* **1990**, *11*, 361−373.

(25) Dubbeldam, D.; Walton, K. S.; Ellis, D. E.; Snurr, R. Q. Exceptional negative thermal expansion in isoreticular metal-organic frameworks. *Angew. Chem. Angew. Chem., Int. Ed.* **2007**, *46*, 4496−4499.

(26) Christenholz, C. L.; Obenchain, D. A.; Peebles, R. A.; Peebles, S. A. Rotational spectroscopic studies of C-H···F interactions in the vinyl fluoride···difluoromethane complex. *J. Phys. Chem. A* **2014**, *118*, 1610−1616.

(27) Abraham, M. J.; Murtola, T.; Schulz, R.; Pall, S.; Smith, J. C.; Hess, B.; Lindahl, E. GROMACS: High performance molecular simulations through multi-level parallelism from laptops to supercomputers. *SoftwareX* **2015**, *1-2*, 19−25.

(28) Mark, P.; Nilsson, L. Structure and dynamics of the TIP3P, SPC, and SPC/E water models at 298 K. *J. Phys. Chem. A* **2001**, *105*, 9954−9960.
(29) Hess, B. P LINCS: A parallel linear constraint solver for molecular simulation. *J. Chem. Theory Comput.* **2008**, *4*, 116−122.
(30) Essmann, U.; Perera, L.; Berkowitz, M. L.; Darden, T.; Lee, H.; Pedersen, L. G. A smooth particle mesh Ewald method. *J. Chem. Phys.* **1995**, *103*, 8577−8593.
(31) Bussi, G.; Donadio, D.; Parrinello, M. Canonical sampling through velocity rescaling. *J. Chem. Phys.* **2007**, *126*, 014101.
(32) Matak, M. Y.; Moghaddam, M. E. The role of short-range Cys171-Cys178 disulfide bond in maintaining cutinase active site integrity: A molecular dynamics simulation. *Biochem. Biophys. Res. Commun.* **2009**, *390*, 201−204.
(33) Longhi, S.; Czjzek, M.; Lamzin, V.; Nicolas, A.; Cambillau, C. Atomic resolution (1.0 A) crystal structure of *Fusarium solani* cutinase: Stereochemical analysis. *J. Mol. Biol.* **1997**, *268*, 779−799.
(34) Su, L.; Chen, S.; Yi, L.; Woodard, R. W.; Chen, J.; Wu, J. Extracellular overexpression of recombinant *Thermobifida fusca* cutinase by alpha-hemolysin secretion system in *E. coli* BL21 (DE3). *Microb. Cell Fact.* **2012**, *11*, 8−14.
(35) Heinig, M.; Frishman, D. STRIDE: A web server for secondary structure assignment from known atomic coordinates of proteins. *Nucleic Acids Res.* **2004**, *32*, W500−W502.
(36) Sokalingam, S.; Madan, B.; Raghunathan, G.; Lee, S. *In silico* study on the effect of surface lysines and arginines on the electrostatic interactions and protein stability. *Biotechnol. Bioprocess Eng.* **2013**, *18*, 18−26.
(37) Armstrong, C. T.; Mason, P. E.; Anderson, J. L. R.; Dempsey, C. E. Arginine side chain interactions and the role of arginine as a gating charge carrier in voltage sensitive ion channels. *Sci. Rep.* **2016**, *6*, 1−10.
(38) Borders, C. L.; Broadwater, J. A.; Bekeny, P. A.; Salmon, J. E.; Lee, A. E.; Eldridge, A. M.; Pett, V. B. A structural role for arginine in proteins: Multiple hydrogen bonds to backbone carbonyl oxygens. *Protein Sci.* **1994**, *3*, 541−548.
(39) Strub, C.; Alies, C.; Lougarre, A.; Ladurantie, C.; Czaplicki, J.; Fournier, D. Mutation of exposed hydrophobic amino acids to arginine to increase protein stability. *BMC Biochem.* **2004**, *5*, 1−6.
(40) Jelesarov, I.; Karshikoff, A. *Protein Structure, Stability, and Interactions*; Shriver, J. W., Ed.; Humana Press: New York, NY, 2009; Vol. *490*, pp 227−260.
(41) Gallivan, J. P.; Dougherty, D. A. Cation-π interactions in structural biology. *Proc. Natl. Acad. Sci. U. S. A.* **1999**, *96*, 9459−9464.

https://dx.doi.org/10.1021/acs.jpcb.0c02145
J. Phys. Chem. B XXXX, XXX, XXX−XXX